

# An Effective Model of the Retinoic Acid Induced HL-60 Differentiation Program

Ryan Tasseff, Holly A. Jensen, Wei Dai, Rodica P. Bunaciu<sup>†</sup>, Johanna Congleton<sup>†</sup>, Andrew Yen<sup>†</sup>, and Jeffrey D. Varner\*

Robert Frederick Smith School of Chemical and Biomolecular Engineering and <sup>†</sup>Department of Biomedical Sciences, Cornell University, Ithaca NY 14853

**Running Title:** Effective modeling of HL-60 differentiation

**To be submitted:** *Frontiers in Systems Biology*

\*Corresponding author:

Jeffrey D. Varner,

Professor, Robert Frederick Smith School of Chemical and Biomolecular Engineering,  
244 Olin Hall, Cornell University, Ithaca NY, 14853

Email: jdv27@cornell.edu

Phone: (607) 255 - 4258

Fax: (607) 255 - 9166

## **Abstract**

In this study, we present an effective model All-Trans Retinoic Acid (ATRA)-induced differentiation of HL-60 cells. The model describes a key architectural feature of ATRA-induced differentiation, positive feedback between an ATRA-inducible signalsome complex involving many proteins including Vav1, a guanine nucleotide exchange factor, and the activation of the mitogen activated protein kinase (MAPK) cascade. The model, which was developed by integrating logical rules with kinetic modeling, was significantly smaller than previous models. However, despite its simplicity, it captured key features of ATRA induced differentiation of HL-60 cells. We identified an ensemble of effective model parameters using measurements taken from ATRA-induced HL-60 cells. Using these parameters, model analysis predicted that MAPK activation was bistable as a function of ATRA exposure. Conformational experiments supported ATRA-induced bistability. These findings, combined with other literature evidence, suggest that positive feedback is central to a diversity of cell fate programs.

## **1 Introduction**

2 Understanding the architecture of differentiation programs is an important therapeutic  
3 challenge. Differentiation induction chemotherapy (DIC), using agents such as the vita-  
4 min A derivative all-trans retinoic acid (ATRA), is a promising approach for the treatment  
5 of many cancers (1–3). For example, ATRA treatment induces remission in 80–90% of  
6 promyelocytic leukemia (APL) PML-RAR $\alpha$ -positive patients (4), thereby transforming a  
7 fatal diagnosis into a manageable disease. However, remission is sometimes not durable  
8 and relapsed cases exhibit emergent ATRA resistance (5, 6). To understand the basis of  
9 this resistance, we must first understand the ATRA-induced differentiation program. To-  
10 ward this challenge, lessons learned in model systems, such as the lineage-uncommitted  
11 human myeloblastic cell line HL-60, could inform our analysis of the more complex dif-  
12 ferentiation programs occurring in patients. Patient derived HL-60 leukemia cells have  
13 been a durable experimental model since the 1970's to study differentiation (7). HL-60  
14 undergoes cell cycle arrest and either myeloid or monocytic differentiation following stim-  
15 ulation; ATRA induces G1/G0-arrest and myeloid differentiation in HL-60 cells, while 1,25-  
16 dihydroxy vitamin D3 (D3) induces arrest and monocytic differentiation. Commitment to  
17 cell cycle arrest and differentiation requires approximately 48 hr of treatment, during which  
18 HL-60 cells undergo two division cycles.

19 Sustained mitogen-activated protein kinase (MAPK) activation is a defining feature of  
20 ATRA-induced HL-60 differentiation. ATRA drives sustained MEK-dependent activation  
21 of the Raf/MEK/ERK pathway, leading to arrest and differentiation (8). MEK inhibition re-  
22 sults in the loss of ERK and Raf phosphorylation, and the failure to arrest and differentiate  
23 (9). ATRA (and its metabolites) are ligands for the hormone activated nuclear transcrip-  
24 tion factors retinoic acid receptor (RAR) and retinoid X receptor (RXR) (10). RAR/RXR  
25 activation is necessary for ATRA-induced Raf phosphorylation (9), and the formation of  
26 an ATRA-inducible signalsome complex at the membrane which drives MAPK activation

27 through a yet to be identified kinase activity. While the makeup of the signalsome com-  
28 plex is not yet known, we do know that it is composed of Src family kinases Fgr and Lyn,  
29 PI3K, c-Cbl, Slp76, and KSR, as well as IRF-1 transcription factors (11–15). Signalsome  
30 formation and activity is driven by ATRA-induced expression of CD38 and the putative  
31 heterotrimeric Gq protein-coupled receptor BLR1 (16, 17). BLR1, identified as an early  
32 ATRA (or D3)-inducible gene using differential display (18), is necessary for MAPK ac-  
33 tivation and differentiation (17), and is also involved with signalsome activity. Studies  
34 of the BLR1 promoter identified a 5' 17bp GT box approximately 1 kb upstream of the  
35 transcriptional start that conferred ATRA responsiveness (17). Members of the BLR1  
36 transcriptional activator complex, e.g. NFATc3 and CREB, are phosphorylated by ERK,  
37 JNK or p38 MAPK family members suggesting positive feedback between the signal-  
38 some and MAPK activation (19). BLR1 overexpression enhanced Raf phosphorylation  
39 and accelerated terminal differentiation, while Raf inhibition reduced BLR1 expression  
40 and differentiation (20). BLR1 knock-out cells failed to activate Raf or differentiate in  
41 the presence of ATRA (20). Interestingly, both the knockdown or inhibition of Raf, also  
42 reduced BLR1 expression and functional differentiation (20). Thus, the expression of  
43 signalsome components e.g., BLR1 was Raf dependent, while Raf activation depended  
44 upon the siganlsome. A recent computational study of ATRA-induced differentiation in  
45 HL-60 cells suggested that the BLR1-MAPK positive feedback circuit was sufficient to ex-  
46 plain ATRA-induced sustained MAPK activation, and the expression of a limited number  
47 of functional differentiation markers (21). Model analysis also suggested that Raf was the  
48 most distinct of the MAPK proteins. However, this previous study developed and analyzed  
49 a complex model, thus leaving open the critical question of what is the minimal positive  
50 feedback circuit required to drive ATRA-induced differentiation.

51 In this study, we explored this question using a minimal mathematical model of the  
52 key architectural feature of ATRA induced differentiation of HL-60 cells, namely positive

53 feedback between an ATRA-inducible signalsome complex and MAPK activation. The  
54 ATRA responsive signalsome-MAPK circuit was then used to drive a downstream gene  
55 expression program which encoded for the expression of functional differentiation mark-  
56 ers. The effective model used a novel framework which integrated logical rules with ki-  
57 netic modeling to describe gene expression and protein regulation, while largely relying  
58 upon biophysical parameters from the literature. This formulation significantly reduced  
59 the size and complexity of the model compared to the previous study of Tasseff et al.,  
60 while increasing the breadth of the biology described (21). The effective model, despite  
61 its simplicity, captured key features of ATRA induced differentiation of HL-60 cells. Model  
62 analysis predicted the bistability of MAPK activation as a function of ATRA exposure; con-  
63 formational experiments supported ATRA-induced bistability. Model simulations were also  
64 consistent with measurements of the influence of MAPK inhibitors, and the failure of BLR1  
65 knockout cells to differentiate when exposed to ATRA. Lastly, we showed by through im-  
66 munoprecipitation studies, that the guanine nucleotide exchange factor Vav1 is potentially  
67 a new ATRA-inducible member of the siganlsome complex. Taken together, these findings  
68 when combined with other literature evidence, suggested that positive feedback architec-  
69 tures are central to differentiation programs generally, and necessary for ATRA-induced  
70 differentiation.

71 **Results**

72 Interrogation of the Raf interactome suggested Vav1 was involved with ATRA-induced  
73 initiation of MAPK activity (Fig. 1). The architecture ultimately responsible for mediating  
74 ATRA-induced Raf activation is not clear. To explore this question, we conducted immuno-  
75 precipitation and subsequent Western blotting to identify physical interactions between  
76 Raf and 19 putative interaction partners. A panel of 19 possible Raf interaction partners  
77 (kinases, GTPases, scaffolding proteins etc) was constructed based upon known signal-  
78 ing pathways. We did not consider the most likely binding partner, the small GTPase  
79 RAS, as previous studies have ruled it out in MAPK activation in HL-60 cells (20, 22).  
80 Total Raf was used as a bait protein for the immunoprecipitation studies. Western blot  
81 analysis using total Raf and pS621 Raf specific antibodies confirmed the presence of the  
82 bait protein, total and phosphorylated forms, in the immunoprecipitate (Fig. 1A). Of the  
83 19 proteins sampled, Vav1, Src, CK2, Akt, and 14-3-3 precipitated with Raf, suggesting a  
84 direct physical interaction was possible. However, only the associations between Raf and  
85 Vav1 and Raf and Src were ATRA-inducible (Fig. 1). Furthermore, the Vav1 and Src as-  
86 sociations were correlated with pS621 Raf abundance in the precipitate. Others proteins  
87 e.g., CK2, Akt and 14-3-3, generally bound Raf regardless of phosphorylation status or  
88 ATRA treatment. The remaining 14 proteins were expressed in whole cell lysate (Fig. 1B),  
89 but were not detectable in the precipitate of Raf IP. Treatment with the Raf kinase inhibitor  
90 GW5074 following ATRA exposure reduced the association of both Vav1 with Raf and  
91 Src with Raf (Fig. 1), although the signal intensity for Src was notably weak. However,  
92 GW5074 did not influence the association of CK2 or 14-3-3 with Raf, further demonstrat-  
93 ing their independence from Raf phosphorylation. Interestingly, the Raf-Akt interaction  
94 qualitatively increased following treatment with GW5074; however, it remained unaffected  
95 by treatment with ATRA. Src family kinases are known to be important in myeloid differ-  
96 entiation (23) and their role in HL-60 differentiation has been investigated elsewhere (11).

Given the existing work and variable reproducibility in the context of the Raf immunoprecipitate, we will not investigate the role of Src further in this study. Taken together, the immunoprecipitation and GW5074 results implicated Vav1 association to be correlated with Raf activation following ATRA-treatment. Previous studies demonstrated that a Vav1-Slp76-Cbl-CD38 complex plays an important role in ATRA-induced MAPK activation and differentiation of HL-60 cells (13). Here we did not observe direct interaction of Raf with Cbl or Slp76; however, this complex could be involved upstream.

Inhibition of Raf kinase activity modulated MAPK activation and differentiation markers following ATRA exposure (Fig. 1D-F). Next, we considered the effect of the Raf kinase inhibitor GW5074 on functional markers of ATRA-induced growth arrest and differentiation. ATRA treatment alone statistically significantly increased the G1/G0 percentage over the untreated control, while GW5074 alone had a negligible effect on the cell cycle distribution (Fig. 1D). Surprisingly, the combination of GW5074 and ATRA statistically significantly increased the G1/G0 population ( $82 \pm 1\%$ ) compared with ATRA alone ( $61 \pm 0.5\%$ ). Increased G1/G0 arrest following the combined treatment with GW5074 and ATRA was unexpected, as the combination of ATRA and the MEK inhibitor (PD98059) has been shown previously to decrease ATRA-induced growth arrest (8). However, growth arrest is not the sole indication of functional differentiation. Expression of the cell surface marker CD11b has also been shown to coincide with HL-60 cells myeloid differentiation (24). We measured CD11b expression, for the various treatment groups, using immunofluorescence flow cytometry 48 hr post-treatment. As with G1/G0 arrest, ATRA alone increased CD11b expression over the untreated control, while GW5074 further enhanced ATRA-induced CD11b expression (Fig. 1E). GW5074 alone had no statistically significant effect on CD11b expression, compared with the untreated control. Lastly, the inducible reactive oxygen species (ROS) response was used as a functional marker of differentiated neutrophils (16). We measured the ROS response induced by the phorbol ester 12-O-

123 tetradecanoylphorbol-13-acetate (TPA) using flow cytometry. Untreated cells showed no  
124 discernible TPA response, with only  $7.0 \pm 3.0\%$  ROS induction (Fig. 1F). Cells treated  
125 with ATRA had a significantly increased TPA response,  $53 \pm 7\%$  ROS induction 48 hr  
126 post-treatment. Treatment with both ATRA and GW5074 statistically significantly reduced  
127 ROS induction ( $22 \pm 0.6\%$ ) compared to ATRA alone. Interestingly, Western blot analy-  
128 sis did not detect a GW5074 effect on ATRA-induced expression of p47phox, a required  
129 upstream component of the ROS response (Fig. 1F, bottom). Thus, the inhibitory effect  
130 of GW5074 on inducible ROS might occur downstream of p47phox expression. How-  
131 ever, the ROS producing complex is MAPK dependent, therefore it is also possible that  
132 GW5074 inhibited ROS production by interfering with MAPK activation (in which case the  
133 p47Phox marker might not accurately reflect phenotypic conversion and differentiation).

134 We constructed an effective model of the ATRA-induced HL-60 differentiation circuit  
135 which described signaling and gene expression events following the addition of ATRA  
136 (Fig. 2). The model connectivity was developed from literature and the studies presented  
137 here. The signaling model recapitulated sustained signalsome/MAPK activation following  
138 exposure to  $1\mu\text{M}$  ATRA (Fig. 3A-B). An ensemble of effective model parameters was es-  
139 timated by minimizing the difference between simulations and time-series measurements  
140 of BLR1 mRNA and cRaf-pS621 following the addition of  $1\mu\text{M}$  ATRA. We focused on the  
141 S621 phosphorylation site of cRaf since enhanced phosphorylation at this site is a defin-  
142 ing characteristic of sustained MAPK activation in HL-60. The effective model captured  
143 both ATRA-induced BLR1 expression (Fig. 3A) and sustained phosphorylation of cRaf-  
144 pS621 (Fig. 3B) in a growing population of HL-60 cells. However, the effective model  
145 failed to capture the decline of BLR1 message after 48 hr of ATRA exposure. Next, we  
146 tested the response of the signalsome/MAPK signaling model to different ATRA dosages.

147 The signalsome/MAPK signaling model was bistable with respect to ATRA induction  
148 (Fig. 3C-D). Nullcline analysis predicted two stable steady-states and a single unstable

state when ATRA was present below a critical threshold (Fig. 3C). In the lower stable state, neither the signalsome nor cRaf-pS621 were present (thus, the differentiation program was deactivated). However, at the high stable state, both the signalsome and cRaf-pS621 were present, allowing for sustained activation and differentiation. Interestingly, when ATRA was above a critical threshold, only the activated state was accessible (Fig. 3D). To test these findings, we first identified the ATRA threshold. We exposed HL-60 cells to different ATRA concentrations for 72 hr (Fig. 3E). Morphological changes associated with differentiation were visible for ATRA  $\geq 0.25 \mu\text{M}$ , suggesting the critical ATRA threshold was near this concentration. Next, we conducted washout ATRA washout experiments to determine if activated cells remained activated even in the absence of ATRA. HL-60 cells locked into an activated state remained activated following ATRA withdraw (Fig. 4). Sustained activation resulted from reinforcing feedback between the signalsome and the MAPK pathway. Thus, following activation, if we inhibited or removed elements from the effective circuit we expected the signalsome and MAPK signals to decay. We simulated ATRA induced activation in the presence of kinase inhibitors, and without key circuit elements. Consistent with experimental results using multiple MAPK inhibitors, ATRA activation in the presence of MAPK inhibitors lowered the steady-state value of signalsome (Fig. 4A). In the presence of BLR1, the signalsome and cRaf-pS621 signals were maintained following ATRA withdraw (Fig. 4B, blue). On the other hand, BLR1 deletion removed the ability of the circuit to maintain a sustained MAPK response following the withdraw of ATRA (Fig. 4B, gray). Lastly, washout experiments in which cells were exposed to 1  $\mu\text{M}$  ATRA for 24 hr, and then transferred to fresh media without ATRA, confirmed the persistence of the self sustaining activated state for up to 144 hr (Fig. 4C). Thus, these experiments and simulations confirmed that reinforcing positive feedback likely drives the ATRA-induced differentiation program. Next, we analyzed the ATRA-induced downstream gene expression program following signalsome and cRaf activation.

175 The reduced order gene expression model described signal integration and ATRA-  
176 induced gene expression events in wild-type HL-60 cells (Fig. 5). The signalsome-MAPK  
177 model produced two outputs, Trigger and cRaf-S621 which drove the downstream dif-  
178 ferentiation program. In particular, Trigger, which is a surrogate for the RAR $\alpha$ /RXR tran-  
179 scriptional complex, regulated the expression of the transcription factors CCATT/enhancer  
180 binding protein  $\alpha$  (C/EBP $\alpha$ ), PU.1, and EGR1. In turn, these transcription factors, in com-  
181 bination with cRaf-S621, regulated the expression of downstream phenotypic markers  
182 such as CD38, CD11b or P47Phox. We assembled the connectivity of the signal integra-  
183 tion program driven by Trigger, and the phenotypic program from literature (supplemental  
184 materials). We estimated the parameters of the signal integration and phenotype pro-  
185 grams from previous studies which contained both steady-state and dynamic measure-  
186 ments of transcription factor and phenotypic marker expression following the addition of  
187 ATRA [REFHERE]. The model simulations captured the time dependent expression of  
188 both CD38 and CD11b following the addition ATRA (Fig. 5A), and steady-state values for  
189 upstream members of the signal integration unit (Fig. 5B).

190 **Discussion**

191 In this study, we presented an effective model of ATRA-inducible differentiation of HL-60  
192 cells which encoded positive feedback between the ATRA-inducible signalsome complex  
193 and the MAPK pathway. Despite its simplicity, the model captured key features of the  
194 ATRA induced differentiation such as sustained MAPK activation, and bistability with re-  
195 spect to ATRA exposure. We also reported a new ATRA-inducible component of the  
196 signalsome, Vav1. Vav1 is a guanine nucleotide exchange factor for Rho family GTPases  
197 that activate pathways leading to actin cytoskeletal rearrangements and transcriptional al-  
198 terations (25). The Vav1/Raf association correlated with Raf activity, was ATRA-inducible  
199 and decreased after treatment with GW5074. The presence of Vav1 in Raf/Grb2 com-  
200 plexes has been shown to correlate with increased Raf activity in mast cells (26). Fur-  
201 thermore, studies on Vav1 knockout mice demonstrated that the loss of Vav1 resulted  
202 in deficiencies of ERK signaling for both T-cells as well as neutrophils (27, 28). While its  
203 function in the signalsome is unclear, Vav1 has been shown to associate with a Cbl-Slp76-  
204 CD38 complex in an ATRA-dependent manner; furthermore, transfection of HL-60 cells  
205 with Cbl mutants that fail to bind CD38, yet still bind Slp76 and Vav1, prevented ATRA-  
206 induced MAPK activation (13). Thus, interaction of Cbl-Slp76-Vav1 and CD38 appears to  
207 be required for transmission of the ATRA signal by the signalsome.

208 We conducted immunoprecipitation studies and identified a limited number of ATRA-  
209 dependent and -independent Raf interaction partners. While we were unable to detect  
210 the association of Raf with common kinases and GTPases such as PKC, PKA, p38, Rac  
211 and Rho, we did establish potential interactions between Raf and key partners such as  
212 Vav1, Src, Akt, CK2 and 14-3-3. All of these partners are known to be associated with Raf  
213 activation or function. Src is known to bind Raf through an SH2 domain, and this associ-  
214 ation has been shown to be dependent of the serine phosphorylation of Raf (29). Thus,  
215 an ATRA inducible Src/Raf association may be a result of ATRA-induced Raf phospho-

216 phosphorylation at S259 or S621. We also identified an interaction between Raf and the Ser/Thr  
217 kinases Akt and CK2. Akt can phosphorylate Raf at S259, as demonstrated by studies  
218 in a human breast cancer line (30). CK2 can also phosphorylate Raf, although the lit-  
219 erature has traditionally focused on S338 and not S621 or S259(31). However, neither  
220 of these kinase interactions were ATRA-inducible, suggesting their association with Raf  
221 alone was not associated with ATRA-induced Raf phosphorylation. The adapter protein  
222 14-3-3 was also constitutively associated with Raf. The interaction between Raf and 14-  
223 3-3 has been associated with both S621 and S259 phosphorylation and activity (32).  
224 Additionally, the association of Raf with 14-3-3 not only stabilized S621 phosphorylation,  
225 but also reversed the S621 phosphorylation from inhibitory to activating (33). Finally, we  
226 found that Vav1/Raf association correlated with Raf activity, was ATRA-inducible and de-  
227 creased after treatment with GW5074. The presence of Vav1 in Raf/Grb2 complexes has  
228 been shown to correlate with increased Raf activity in mast cells (26). Furthermore, stud-  
229 ies on Vav1 knockout mice demonstrated that the loss of Vav1 resulted in deficiencies of  
230 ERK signaling for both T-cells as well as neutrophils (27, 28). Interestingly, while an in-  
231 tegrin ligand-induced ROS response was blocked in Vav1 knockout neutrophils, TPA was  
232 able to bypass the Vav1 requirement and stimulate both ERK phosphorylation and ROS  
233 induction (28). In this study, the TPA-induced ROS response was dependent upon Raf  
234 kinase activity, and was mitigated by the addition of GW5074. It is possible that Vav1 is  
235 downstream of various integrin receptors but upstream of Raf in terms of inducible ROS  
236 responses. Vav1 has also been shown to associate with a Cbl-Slp76-CD38 complex in an  
237 ATRA-dependent manner; furthermore, transfection of HL-60 cells with Cbl mutants that  
238 fail to bind CD38, yet still bind Slp76 and Vav1, prevents ATRA-induced MAPK activation  
239 (13). The literature suggest a variety of possible receptor-signaling pathways, which in-  
240 volve Vav1, for MAPK activation; moreover, given the ATRA-inducible association Vav1  
241 may play a direct role in Raf activation.

242 We hypothesized that Vav1 is a member of an ATRA-inducible complex which propels  
243 sustained MAPK activation, arrest and differentiation. Initially, ATRA-induced Vav1 ex-  
244 pression drives increased association between Vav1 and Raf. This increased interaction  
245 facilitates phosphorylation and activation of Raf by pre-bound Akt and/or CK2 at S621  
246 or perhaps S259. Constitutively bound 14-3-3 may also stabilize the S621 phosphory-  
247 lation, modulate the activity and/or up-regulate autophosphorylation. Activated Raf can  
248 then drive ERK activation, which in turn closes the positive feedback loop by activating  
249 Raf transcription factors, e.g. Sp1 and/or STAT1 (34–37). We tested this working hy-  
250 pothesis using mathematical modeling. The model recapitulated both ATRA time-course  
251 data as well as the GW5074 inhibitor effects. This suggested the proposed Raf-Vav1  
252 architecture was at least consistent with the experimental studies. Further, analysis of  
253 the Raf-Vav1 model identified bistability in ppERK levels. Thus, two possible MAPK ac-  
254 tivation branches were possible for experimentally testable ATRA values. The analysis  
255 also suggested the ATRA-induced Raf-Vav1 architecture could be locked into a sustained  
256 signaling mode (high ppERK) even in the absence of a ATRA signal. This locked-in prop-  
257 erty could give rise to an ATRA-induction memory. We validated the treatment memory  
258 property predicted by the Raf-Vav1 circuit experimentally using ATRA-washout experi-  
259 ments. ERK phosphorylation levels remained high for more then 96 hr after ATRA was  
260 removed. Previous studies demonstrated that HL-60 cells possessed an inheritable mem-  
261 ory of ATRA stimulus (38). Although the active state was self-sustaining, the inactive state  
262 demonstrated considerable robustness to perturbation. For example, we found that 50x  
263 overexpression of Raf was required to reliably lock MAPK into the activated state, while  
264 small perturbations had almost no effect on ppERK levels over the entire ensemble. CD38  
265 expression correlated with the ppERK, suggesting its involvement in the signaling com-  
266 plex. Our computational and experimental results showed that positive feedback, through  
267 ERK-dependent Raf expression, could sustain MAPK signaling through many division cy-

268 cles. Such molecular mechanisms could underly aspects of cellular memory associated  
269 to consecutive ATRA treatments.

270 Several engineered, or naturally occurring systems involved in cell fate decisions incor-  
271 porate positive feedback and bistability (39). One of the most well studied cell fate circuits  
272 is the Mos mitogen-activated protein kinase cascade in *Xenopus* oocytes. This cascade  
273 is activated when oocytes are induced by the steroid hormone progesterone (40). The  
274 MEK-dependent activation of p42 MAPK stimulates the accumulation of the Mos onco-  
275 protein, which in turn activates MEK, thereby closing the feedback loop. This is similar to  
276 the differentiation circuit presented here; ATRA drives signalsome which activates MAPK,  
277 cell-cycle arrest, differentiation and signalsome. Thus, while HL-60 and *Xenopus* oocytes  
278 are vastly different biological models, they share similar cell fate decision architectures.  
279 Other unrelated cell fate decisions such as programmed cell death have also been sug-  
280 gested to be bistable (41). Still more biochemical networks important to human health,  
281 for example the human coagulation or complement cascades, also feature strong positive  
282 feedback elements (42). Thus, while positive feedback is sometimes not desirable in man-  
283 made systems, it may be at the core of a diverse variety of cell fate programs and other  
284 networks important to human health.

285 Model performance was impressive given its limited size. However, there were several  
286 issues to explore further. First, there was likely missing connectivity in the effective differ-  
287 entiation circuit. Decreasing BLR1 expression with simultaneously sustained cRaf-pS261  
288 activation was not captured by the current network architecture. This suggested that  
289 signalsome, once activated, had a long lifetime as decreased BLR1 expression did not  
290 impact cRaf-pS261 abundance. We could model this by separating signalsome formation  
291 into an inactive precursor pool that is transformed to a long-lived activated signalsome by  
292 MAPK activation. We should also explore adding additional downstream biological mod-  
293 ules to this skeleton model, for example the upregulation of reactive oxygen markers such

<sup>294</sup> as p47Phox or cell cycle arrest components to capture the switch from an actively prolif-  
<sup>295</sup> erating population to a population in G0-arrest. Next, the choice of max/min integration  
<sup>296</sup> rules or the particular form of the transfer functions could also be explored. Integration  
<sup>297</sup> rules other than max/min could be used, such as the mean or the product, assuming the  
<sup>298</sup> range of the transfer functions is always  $f \in [0, 1]$ . Alternative integration rules might  
<sup>299</sup> have different properties which could influence model identification or performance. For  
<sup>300</sup> example, a mean integration rule would be differentiable, allowing derivative-based opti-  
<sup>301</sup> mization approaches to be used. The form of the transfer function could also be explored.  
<sup>302</sup> We choose hill-like functions because of their prominence in the systems and synthetic  
<sup>303</sup> biology community. However, many other transfer functions are possible.

304 **Materials and Methods**

305 *Effective ATRA differentiation model.* ATRA induced signaling events were modeled us-  
 306 ing saturation kinetics within an ordinary differential equation (ODE) framework:

$$\frac{1}{\tau_i} \frac{dx_i}{dt} = \sum_{j=1}^{\mathcal{R}} \sigma_{ij} r_j(\mathbf{x}, \epsilon, \mathbf{k}) - (\mu + k_d) x_i \quad i = 1, 2, \dots, \mathcal{M} \quad (1)$$

307 The quantity  $x_i$  denotes concentration of signaling species  $i$ , while  $\mathcal{R}$  and  $\mathcal{M}$  denote the  
 308 number of signaling reactions and signaling species in the model, respectively. The quan-  
 309 tity  $\tau_i$  denotes a time scale parameter for species  $i$  which captures un-modeled effects; in  
 310 the current study  $\tau_i = 1$  for all species. The quantity  $r_j(\mathbf{x}, \epsilon, \mathbf{k})$  denotes the rate of pro-  
 311 cess  $j$ . Typically, process  $j$  is a non-linear function of biochemical and enzyme species  
 312 abundance, as well as unknown model parameters  $\mathbf{k}$  ( $\mathcal{K} \times 1$ ). The quantity  $\sigma_{ij}$  denotes the  
 313 stoichiometric coefficient for species  $i$  in reaction  $j$ . If  $\sigma_{ij} > 0$ , species  $i$  is produced by  
 314 reaction  $j$ . Conversely, if  $\sigma_{ij} < 0$ , species  $i$  is consumed by reaction  $j$ , while  $\sigma_{ij} = 0$  indi-  
 315 cates species  $i$  is not connected with reaction  $j$ . Lastly,  $\mu$  denotes the specific growth rate,  
 316 and  $k_d$  denotes the rate constant controlling cell death. Species balances were subject to  
 317 the initial conditions  $\mathbf{x}(t_o) = \mathbf{x}_o$ .

318 Signaling rate processes were written as the product of a kinetic term ( $\bar{r}_j$ ) and a control  
 319 term ( $v_j$ ) in the HL-60 model. The rate of an enzyme catalyzed process was modeled  
 320 using saturation kinetics:

$$\bar{r}_j = k_j \epsilon_i \prod_{s \in m_j^-} \left( \frac{x_s}{K_{js} + x_s} \right) \quad (2)$$

321 where  $k_j$  denotes the catalytic rate constant for reaction  $j$ ,  $\epsilon_i$  denotes the abundance of the  
 322 enzyme catalyzing reaction  $j$ , and  $K_{js}$  denotes the saturation constant for species  $s$  and  
 323  $s \in m_j$  denotes the set of *reactants* for reaction  $j$ . The control terms  $0 \leq v_j \leq 1$  depended  
 324 upon the combination of factors which influenced rate process  $j$ . For each rate, we used

325 a rule-based approach to select from competing control factors. If rate  $j$  was influenced  
 326 by  $1, \dots, m$  factors, we modeled this relationship as  $v_j = \mathcal{I}_j(f_{1j}(\cdot), \dots, f_{mj}(\cdot))$  where  
 327  $0 \leq f_{ij}(\cdot) \leq 1$  denotes a regulatory transfer function quantifying the influence of factor  $i$   
 328 on rate  $j$ . The function  $\mathcal{I}_j(\cdot)$  is an integration rule which maps the output of regulatory  
 329 transfer functions into a control variable. In this study, we used  $\mathcal{I}_j \in \{\min, \max\}$  and hill  
 330 transfer functions (43). If a process had no modifying factors,  $v_j = 1$ .

331 The HL-60 model described both signal transduction and gene expression events fol-  
 332 lowing the addition of ATRA. The output of the signal transduction model was the input to  
 333 the gene expression model. For each gene  $j = 1, 2, \dots, \mathcal{G}$ , we modeled both the mRNA  
 334 ( $m_j$ ) and protein ( $p_j$ ):

$$\frac{dm_j}{dt} = r_{T,j} - (\mu + \theta_{m,j}) m_j + \lambda_j \quad (3)$$

$$\frac{dp_j}{dt} = r_{X,j} - (\mu + \theta_{p,j}) p_j \quad (4)$$

335 The terms  $r_{T,j}$  and  $r_{X,j}$  denote the specific rates of transcription, and translation while  
 336 the terms  $\theta_{m,j}$  and  $\theta_{p,j}$  denote first-order degradation constants for mRNA and protein,  
 337 respectively. The specific transcription rate was modeled as the product of a kinetic term  
 338  $\bar{r}_{T,j}$  and a control term  $u_j$  which described how the abundance of transcription factors, or  
 339 other regulators influenced the expression of gene  $j$ . The kinetic rate of transcription was  
 340 modeled as:

$$\bar{r}_{T,j} = V_T^{\max} \left( \frac{L_{T,o}}{L_{T,j}} \right) \left( \frac{G_j}{K_T + G_j} \right) \quad (5)$$

341 where the maximum gene expression rate  $V_T^{\max}$  was defined as the product of a char-  
 342 acteristic transcription rate constant ( $k_T$ ) and the abundance of RNA polymerase ( $R_1$ ),  
 343  $V_T^{\max} = k_T (R_1)$ . The  $(L_{T,o}/L_{T,j})$  term denotes the ratio of transcription read lengths,  
 344 where  $L_{T,o}$  is a characteristic gene length, and  $L_{T,j}$  denotes the length of gene  $j$ . Thus,  
 345 the  $(L_{T,o}/L_{T,j})$  term is gene specific correction to the characteristic transcription rate. The

346 degradation rate constants were defined as  $\theta_{m,j}$  and  $\theta_{p,j}$  denote characteristic degradation  
 347 constants for mRNA and protein, respectively.

348 The gene expression control term  $0 \leq u_j \leq 1$  depended upon the combination of  
 349 factors which influenced rate process  $j$ . If the expression of gene  $j$  was influenced  
 350 by  $1, \dots, m$  factors, we modeled this relationship as  $u_j = \mathcal{I}_j(f_{1j}(\cdot), \dots, f_{mj}(\cdot))$  where  
 351  $0 \leq f_{ij}(\cdot) \leq 1$  denotes a regulatory transfer function quantifying the influence of factor  
 352  $i$  on the expression of gene  $j$ , and  $\mathcal{I}_j(\cdot)$  denotes an integration rule. In this study, the  
 353 integration rule governing gene expression was the weighted fraction of promoter config-  
 354 urations resulting in gene expression. Thus, the control variable  $u_j$  took the form:

$$u_j = \frac{W_{R_{1,j}} + \sum_n W_{nj} f_{nj}}{1 + W_{R_{1,j}} + \sum_d W_{dj} f_{dj}} \quad (6)$$

355 where the numerator, the weighted sum (with weights  $W_{nj}$ ) of promoter configurations  
 356 leading to gene expression, was normalized by all possible promoter configurations. The  
 357 likelihood of each configuration was quantified by the transfer function  $f_{nj}$  (which we mod-  
 358 eled using hill like functions), while the lead term in the numerator  $W_{R_{1,j}}$  denotes the  
 359 weight of constitutive expression for gene  $j$ . If a gene expression process had no modify-  
 360 ing factors,  $u_j = 1$ . Lastly, the specific translation rate was modeled as:

$$r_{X,j} = V_X^{\max} \left( \frac{m_j}{K_X + m_j} \right) \quad (7)$$

361 where  $V_X^{\max}$  denotes a characteristic maximum translation rate estimated from literature,  
 362 and  $K_X$  denotes a translation saturation constant. The characteristic maximum translation  
 363 rate was defined as the product of a characteristic translation rate constant ( $k_X$ ) and the  
 364 Ribosome abundance ( $R_2$ ),  $V_X^{\max} = k_X (R_2)$ .

365 In this study, we estimated the  $W_{ij}$  parameters, and the parameters in the trans-

366 fer functions  $f_{dj}$  from gene expression data sets. On the other hand, we estimated  
 367  $k_T, k_X, \theta_{m,j}, \theta_{p,j}, R_1$  and  $R_2$  using estimates of transcription and translation rates, the half-  
 368 life of a typical mRNA and protein, and a typical value for the copies per cell of RNA  
 369 polymerase and ribosomes from literature (44). The saturation constants  $K_X$  and  $K_T$   
 370 were adjusted so that gene expression and translation resulted in gene products on a bio-  
 371 logically realistic concentration scale. Lastly, we calculated the concentration for gene  $G_j$   
 372 by assuming, on average, that a cell had two copies of each gene at any given time. Thus,  
 373 the bulk of our gene expression parameters were based directly upon literature values,  
 374 and were not adjusted during model identification. The values used for the characteris-  
 375 tic transcription/translation parameters, degradation constants and macromolecular copy  
 376 number are given in the supplemental materials along with the specific formulas required  
 377 to calculate all derived constants.

378 *Estimation of signaling and gene expression model parameters.* Signal and gene ex-  
 379 pression model parameters were estimated by minimizing the squared difference between  
 380 simulations and experimental data set  $j$ :

$$E_j(\mathbf{k}) = \sum_{i=1}^{\mathcal{T}_j} \left( \hat{\mathcal{M}}_{ij} - \hat{y}_{ij}(\mathbf{k}) \right)^2 + \left( \frac{\mathcal{M}'_{ij} - \max y_{ij}}{\mathcal{M}'_{ij}} \right)^2 \quad (8)$$

381 The terms  $\hat{\mathcal{M}}_{ij}$  and  $\hat{y}_{ij}$  denote scaled experimental observations and simulation outputs  
 382 at time  $i$  from training set  $j$ , where  $\mathcal{T}_j$  denoted the number of time points for data set  $j$ .  
 383 The first term in Eqn. (8) quantified the relative simulation error. We used immunoblot  
 384 intensity measurements for model training. Thus, we trained the model on the *relative*  
 385 change between bands within each data set. Suppose we have the intensity of species  $x$   
 386 at time  $\{t_1, t_2, \dots, t_n\}$  in condition  $j$ . The scaled value  $0 \leq \hat{\mathcal{M}}_{ij} \leq 1$  is given by:

$$\hat{\mathcal{M}}_{ij} = \left( \mathcal{M}_{ij} - \min_i \mathcal{M}_{ij} \right) / \left( \max_i \mathcal{M}_{ij} - \min_i \mathcal{M}_{ij} \right) \quad (9)$$

387 where  $\hat{M}_{ij} = 0$  and  $\hat{M}_{ij} = 1$  describe the lowest (highest) intensity bands. A similar  
388 scaling was used for the simulation output. The second term in the objective function  
389 ensured a realistic concentration scale was estimated by the model. We set the highest  
390 intensity band to  $M'_{ij} = 10$  [AU] for all simulations. We minimized the total model residual  
391  $\sum_j E_j$  using heuristic optimization starting from a random initial parameter guess.

392 The signaling and gene expression model equations were implemented in Julia and  
393 solved using the CVODE routine of the Sundials package (45, 46). The model code and  
394 parameter ensemble is freely available under an MIT software license and can be down-  
395 loaded from <http://www.varnerlab.org>.

396 *Cell culture and treatment* Human myeloblastic leukemia cells (HL-60 cells) were grown  
397 in a humidified atmosphere of 5% CO<sub>2</sub> at 37°C and maintained in RPMI 1640 from Gibco  
398 (Carlsbad, CA) supplemented with 5% heat inactivated fetal bovine serum from Hyclone  
399 (Logan, UT) and 1× antibiotic/antimicotic (Gibco, Carlsbad, CA). Cells were cultured in  
400 constant exponential growth (47). Experimental cultures were initiated at  $0.1 \times 10^6$  cells/mL  
401 24 hr prior to ATRA treatment; if indicated, cells were also treated with GW5074 (2 $\mu$ M) 18  
402 hr before ATRA treatment. For the cell culture washout experiments, cells were treated  
403 with ATRA for 24 hr, washed 3x with prewarmed serum supplemented culture medium  
404 to remove ATRA, and reseeded in ATRA-free media as described. Western blot analysis  
405 was performed at incremental time points after removal of ATRA.

406 *Chemicals* All-Trans Retinoic Acid (ATRA) from Sigma-Aldrich (St. Louis, MO) was dis-  
407 solved in 100% ethanol with a stock concentration of 5mM, and used at a final concen-  
408 tration of 1 $\mu$ M (unless otherwise noted). The cRaf inhibitor GW5074 from Sigma-Aldrich  
409 (St. Louis, MO) was dissolved in DMSO with a stock concentration of 10mM, and used  
410 at a final concentration of 2 $\mu$ M. HL-60 cells were treated with 2 $\mu$ M GW5074 with or with-  
411 out ATRA (1 $\mu$ M) at 0 hr. This GW5074 dosage had a negligible effect on the cell cycle  
412 distribution, compared to ATRA treatment alone.

413 *Immunoprecipitation and western blotting* Approximately  $1.2 \times 10^7$  cells were lysed using  
414  $400\mu\text{L}$  of M-Per lysis buffer from Thermo Scientific (Waltham, MA). Lysates were cleared  
415 by centrifugation at  $16,950 \times g$  in a micro-centrifuge for 20 min at  $4^\circ\text{C}$ . Lysates were  
416 pre-cleared using  $100\mu\text{L}$  protein A/G Plus agarose beads from Santa Cruz Biotechnology  
417 (Santa Cruz, CA) by inverting overnight at  $4^\circ\text{C}$ . Beads were cleared by centrifugation and  
418 total protein concentration was determined by a BCA assay (Thermo Scientific, Waltham,  
419 MA). Immunoprecipitations were setup by bringing lysate to a concentration of 1g/L in a  
420 total volume of  $300\mu\text{L}$  (M-Per buffer was used for dilution). The anti-Raf antibody was  
421 added at  $3\mu\text{L}$ . A negative control with no bait protein was also used to exclude the di-  
422 rect interaction of proteins with the A/G beads. After 1 hr of inversion at  $4^\circ\text{C}$ ,  $20\mu\text{L}$  of  
423 agarose beads was added and samples were left to invert overnight at  $4^\circ\text{C}$ . Samples  
424 were then washed three times with M-Per buffer by centrifugation. Finally proteins were  
425 eluted from agarose beads using a laemmli loading buffer. Eluted proteins were resolved  
426 by SDS-PAGE and Western blotting. Total lysate samples were normalized by total protein  
427 concentration ( $20\mu\text{g}$  per sample) and resolved by SDS-PAGE and Western blotting. Sec-  
428 ondary HRP bound antibody was used for visualization. All antibodies were purchased  
429 from Cell Signaling (Boston, MA) with the exception of  $\alpha$ -p621 Raf which was purchased  
430 from Biosource/Invitrogen (Carlsbad, CA), and  $\alpha$ -CK2 from BD Biosciences (San Jose,  
431 CA).

432 *Morphology assessment* Untreated and ATRA-treated HL-60 cells were collected after  
433 72 hr and cytocentrifuged for 3 min at 700 rpm onto glass slides. Slides were air-dried  
434 and stained with Wright's stain. Slide images were captured at 40X (Leica DM LB 100T  
435 microscope, Leica Microsystems).

<sup>436</sup> **Competing interests**

<sup>437</sup> The authors declare that they have no competing interests.

<sup>438</sup> **Author's contributions**

<sup>439</sup> J.V and A.Y directed the study. R.T, H.J and J.C conducted the cell culture measurements. J.V and W.D developed the reduced order HL-60 models and the parameter ensemble. W.D analyzed the model ensemble, and generated figures for the manuscript.

<sup>442</sup> The manuscript was prepared and edited for publication by W.D, A.Y and J.V.

<sup>443</sup> **Acknowledgements**

<sup>444</sup> We gratefully acknowledge the suggestions from the anonymous reviewers to improve  
<sup>445</sup> this manuscript.

<sup>446</sup> **Funding**

<sup>447</sup> We acknowledge the financial support to J.V. by the National Science Foundation CA-  
<sup>448</sup> REER (CBET-0846876) for the support of R.T. and H.J. In addition, we acknowledge  
<sup>449</sup> support to A.Y. from the National Institutes of Health (CA 30555, CA152870) and a grant  
<sup>450</sup> from New York State Stem Cell Science. Lastly, we acknowledge the financial support to  
<sup>451</sup> J.V. and A.Y. from the National Cancer Institute (#U54 CA143876). The content is solely  
<sup>452</sup> the responsibility of the authors and does not necessarily represent the official views of  
<sup>453</sup> the National Cancer Institute or the National Institutes of Health.

454 **References**

- 455 1. Bushue N, Wan YJY (2010) Retinoid pathway and cancer therapeutics. *Adv Drug*  
456 *Deliv Rev* 62: 1285-98.
- 457 2. Tang XH, Gudas LJ (2011) Retinoids, retinoic acid receptors, and cancer. *Annu Rev*  
458 *Pathol* 6: 345-64.
- 459 3. Cheung FSG, Lovicu FJ, Reichardt JKV (2012) Current progress in using vitamin d  
460 and its analogs for cancer prevention and treatment. *Expert Rev Anticancer Ther* 12:  
461 811-37.
- 462 4. Nilsson B (1984) Probable in vivo induction of differentiation by retinoic acid of  
463 promyelocytes in acute promyelocytic leukaemia. *Br J Haematol* 57: 365-71.
- 464 5. Warrell RP Jr (1993) Retinoid resistance in acute promyelocytic leukemia: new mech-  
465 anisms, strategies, and implications. *Blood* 82: 1949-53.
- 466 6. Freemantle SJ, Spinella MJ, Dmitrovsky E (2003) Retinoids in cancer therapy and  
467 chemoprevention: promise meets resistance. *Oncogene* 22: 7305-15.
- 468 7. Breitman TR, Selonick SE, Collins SJ (1980) Induction of differentiation of the human  
469 promyelocytic leukemia cell line (HL-60) by retinoic acid. *Proc Natl Acad Sci U S A*  
470 77: 2936–2940.
- 471 8. Yen A, Roberson MS, Varvayanis S, Lee AT (1998) Retinoic acid induced  
472 mitogen-activated protein (MAP)/extracellular signal-regulated kinase (ERK) kinase-  
473 dependent MAP kinase activation needed to elicit HL-60 cell differentiation and  
474 growth arrest. *Cancer Res* 58: 3163–3172.
- 475 9. Hong HY, Varvayanis S, Yen A (2001) Retinoic acid causes MEK-dependent RAF  
476 phosphorylation through RARalpha plus RXR activation in HL-60 cells. *Differentiation*  
477 68: 55–66.
- 478 10. Mangelsdorf DJ, Ong ES, Dyck JA, Evans RM (1990) Nuclear receptor that identifies  
479 a novel retinoic acid response pathway. *Nature* 345: 224–229.

- 480 11. Congleton J, MacDonald R, Yen A (2012) Src inhibitors, PP2 and dasatinib, increase  
481 retinoic acid-induced association of Lyn and c-Raf (S259) and enhance MAPK-  
482 dependent differentiation of myeloid leukemia cells. Leukemia 26: 1180-8.
- 483 12. Shen M, Bunaci R, Congleton J, Jensen H, Sayam L, et al. (2011) Interferon regula-  
484 tory factor-1 binds c-Cbl, enhances mitogen activated protein kinase signaling and  
485 promotes retinoic acid-induced differentiation of HL-60 human myelo-monoblastic  
486 leukemia cells. Leuk Lymphoma 52: 2372-9.
- 487 13. Shen M, Yen A (2009) c-Cbl tyrosine kinase-binding domain mutant G306E abolishes  
488 the interaction of c-Cbl with CD38 and fails to promote retinoic acid-induced cell dif-  
489 ferentiation and G0 arrest. J Biol Chem 284: 25664–25677.
- 490 14. Yen A, Varvayanis S, Smith J, Lamkin T (2006) Retinoic acid induces expression of  
491 SLP-76: expression with c-FMS enhances ERK activation and retinoic acid-induced  
492 differentiation/G0 arrest of HL-60 cells. Eur J Cell Biol 85: 117–132.
- 493 15. Marchisio M, Bertagnolo V, Colamussi ML, Capitani S, Neri LM (1998) Phosphatidyli-  
494 nositol 3-kinase in HL-60 nuclei is bound to the nuclear matrix and increases during  
495 granulocytic differentiation. Biochem Biophys Res Commun 253: 346-51.
- 496 16. Congleton J, Jiang H, Malavasi F, Lin H, Yen A (2011) ATRA-induced HL-60 myeloid  
497 leukemia cell differentiation depends on the CD38 cytosolic tail needed for membrane  
498 localization, but CD38 enzymatic activity is unnecessary. Exp Cell Res 317: 910–  
499 919.
- 500 17. Wang J, Yen A (2004) A novel retinoic acid-responsive element regulates retinoic acid  
501 induced BLR1 expression. Mol Cell Biol 24: 2423 - 2443.
- 502 18. Yen A (1990) HL-60 cells as a model of growth and differentiation: the significance of  
503 variant cells. Hematology Review 4: 5-46.
- 504 19. Yang T, Xiong Q, Enslen H, Davis R, Chow CW (2002) Phosphorylation of NFATc4 by  
505 p38 mitogen-activated protein kinases. Mol Cell Biol 22: 3892–3904.

- 506 20. Wang J, Yen A (2008) A MAPK-positive Feedback Mechanism for BLR1 Signaling  
507 Propels Retinoic Acid-triggered Differentiation and Cell Cycle Arrest. *J Biol Chem*  
508 283: 4375–4386.
- 509 21. Tasseff R, Nayak S, Song S, Yen A, Varner J (2011) Modeling and analysis of retinoic  
510 acid induced differentiation of uncommitted precursor cells. *Integr Biol* 3: 578 - 591.
- 511 22. Katagiri K, Hattori S, Nakamura S, Yamamoto T, Yoshida T, et al. (1994) Activation  
512 of ras and formation of gap complex during tpa-induced monocytic differentiation of  
513 hl-60 cells. *Blood* 84: 1780–1789.
- 514 23. Miranda MB, Johnson DE (2007) Signal transduction pathways that contribute to  
515 myeloid differentiation. *Leukemia* 21: 1363–1377.
- 516 24. Hickstein DD, Back AL, Collins SJ (1989) Regulation of expression of the cd11b and  
517 cd18 subunits of the neutrophil adherence receptor during human myeloid differenti-  
518 ation. *J Biol Chem* 264: 21812–21817.
- 519 25. Hornstein I, Alcover A, Katzav S (2004) Vav proteins, masters of the world of cy-  
520 toskeleton organization. *Cell Signal* 16: 1-11.
- 521 26. Song JS, Gomez J, Stancato LF, Rivera J (1996) Association of a p95 vav-containing  
522 signaling complex with the fcepsilonlonri gamma chain in the rbl-2h3 mast cell line. ev-  
523 idence for a constitutive in vivo association of vav with grb2, raf-1, and erk2 in an  
524 active complex. *J Biol Chem* 271: 26962–26970.
- 525 27. Costello PS, Walters AE, Mee PJ, Turner M, Reynolds LF, et al. (1999) The rho-family  
526 gtp exchange factor vav is a critical transducer of t cell receptor signals to the calcium,  
527 erk, and nf-kappab pathways. *Proc Natl Acad Sci U S A* 96: 3035–3040.
- 528 28. Graham D, Robertson C, Bautista J, Mascarenhas F, Diacovo M, et al. (2007)  
529 Neutrophil-mediated oxidative burst and host defense are controlled by a Vav-  
530 PLCgamma2 signaling axis in mice. *J Clin Invest* 117: 3445–3452.
- 531 29. Cleghon V, Morrison DK (1994) Raf-1 interacts with fyn and src in a non-

- 532 phosphotyrosine-dependent manner. *J Biol Chem* 269: 17749–17755.
- 533 30. Zimmermann S, Moelling K (1999) Phosphorylation and regulation of raf by akt (pro-  
534 tein kinase b). *Science* 286: 1741–1744.
- 535 31. Ritt DA, Zhou M, Conrads TP, Veenstra TD, Copeland TD, et al. (2007) Ck2 is a  
536 component of the ksr1 scaffold complex that contributes to raf kinase activation. *Curr  
537 Biol* 17: 179–184.
- 538 32. Hekman M, Wiese S, Metz R, Albert S, Troppmair J, et al. (2004) Dynamic changes in  
539 c-raf phosphorylation and 14-3-3 protein binding in response to growth factor stimula-  
540 tion: differential roles of 14-3-3 protein binding sites. *J Biol Chem* 279: 14074–14086.
- 541 33. Dhillon AS, Yip YY, Grindlay GJ, Pakay JL, Dangers M, et al. (2009) The c-terminus  
542 of raf-1 acts as a 14-3-3-dependent activation switch. *Cell Signal* 21: 1645–1651.
- 543 34. Kim HS, Lim IK (2009) Phosphorylated extracellular signal-regulated protein kinases  
544 1 and 2 phosphorylate sp1 on serine 59 and regulate cellular senescence via tran-  
545 scription of p21sdi1/cip1/waf1. *J Biol Chem* 284: 15475–15486.
- 546 35. Milanini-Mongiat J, Pouyss?gur J, Pag?o G (2002) Identification of two sp1 phospho-  
547 rylation sites for p42/p44 mitogen-activated protein kinases: their implication in vas-  
548 cular endothelial growth factor gene transcription. *J Biol Chem* 277: 20631–20639.
- 549 36. Zhang Y, Cho YY, Petersen BL, Zhu F, Dong Z (2004) Evidence of stat1 phospho-  
550 rylation modulated by mapks, mek1 and msk1. *Carcinogenesis* 25: 1165–1175.
- 551 37. Li Z, Theus MH, Wei L (2006) Role of erk 1/2 signaling in neuronal differentiation of  
552 cultured embryonic stem cells. *Dev Growth Differ* 48: 513–523.
- 553 38. Yen A, Reece SL, Albright KL (1984) Dependence of hl-60 myeloid cell differentiation  
554 on continuous and split retinoic acid exposures: precommitment memory associated  
555 with altered nuclear structure. *J Cell Physiol* 118: 277–286.
- 556 39. Ferrell J (2002) Self-perpetuating states in signal transduction: positive feedback,  
557 double-negative feedback and bistability. *Curr Opin Cell Biol* 14: 140-8.

- 558 40. Xiong W, Ferrell J (2003) A positive-feedback-based bistable 'memory module' that  
559 governs a cell fate decision. *Nature* 426: 460-5.
- 560 41. Bagci EZ, Vodovotz Y, Billiar TR, Ermentrout GB, Bahar I (2006) Bistability in apop-  
561 tosis: roles of bax, bcl-2, and mitochondrial permeability transition pores. *Biophys J*  
562 90: 1546-59.
- 563 42. Luan D, Zai M, Varner JD (2007) Computationally derived points of fragility of a human  
564 cascade are consistent with current therapeutic strategies. *PLoS Comput Biol* 3:  
565 e142.
- 566 43. Wayman JA, Sagar A, Varner JD (2015) Dynamic modeling of cell-free biochemical  
567 networks using effective kinetic models. *Processes* 3: 138.
- 568 44. Milo R, Jorgensen P, Moran U, Weber G, Springer M (2010) Bionumbers—the  
569 database of key numbers in molecular and cell biology. *Nucleic Acids Res* 38: D750-  
570 3.
- 571 45. Bezanson J, Edelman A, Karpinski S, Shah VB (2014) Julia: A fresh approach to  
572 numerical computing. *CoRR* abs/1411.1607.
- 573 46. Hindmarsh A, Brown P, Grant K, Lee S, Serban R, et al. (2005) Sundials: Suite of non-  
574 linear and differential/algebraic equation solvers. *ACM Transactions on Mathematical  
575 Software* 31: 363-396.
- 576 47. Brooks SC, Kazmer S, Levin AA, Yen A (1996) Myeloid differentiation and retinoblas-  
577 toma phosphorylation changes in HL-60 cells induced by retinoic acid receptor- and  
578 retinoid X receptor-selective retinoic acid analogs. *Blood* 87: 227–237.
- 579 48. Jensen HA, Yourish HB, Bunaciu RP, Varner JD, Yen A (2015) Induced myelomono-  
580 cytic differentiation in leukemia cells is accompanied by noncanonical transcription  
581 factor expression. *FEBS Open Bio* 5: 789-800.

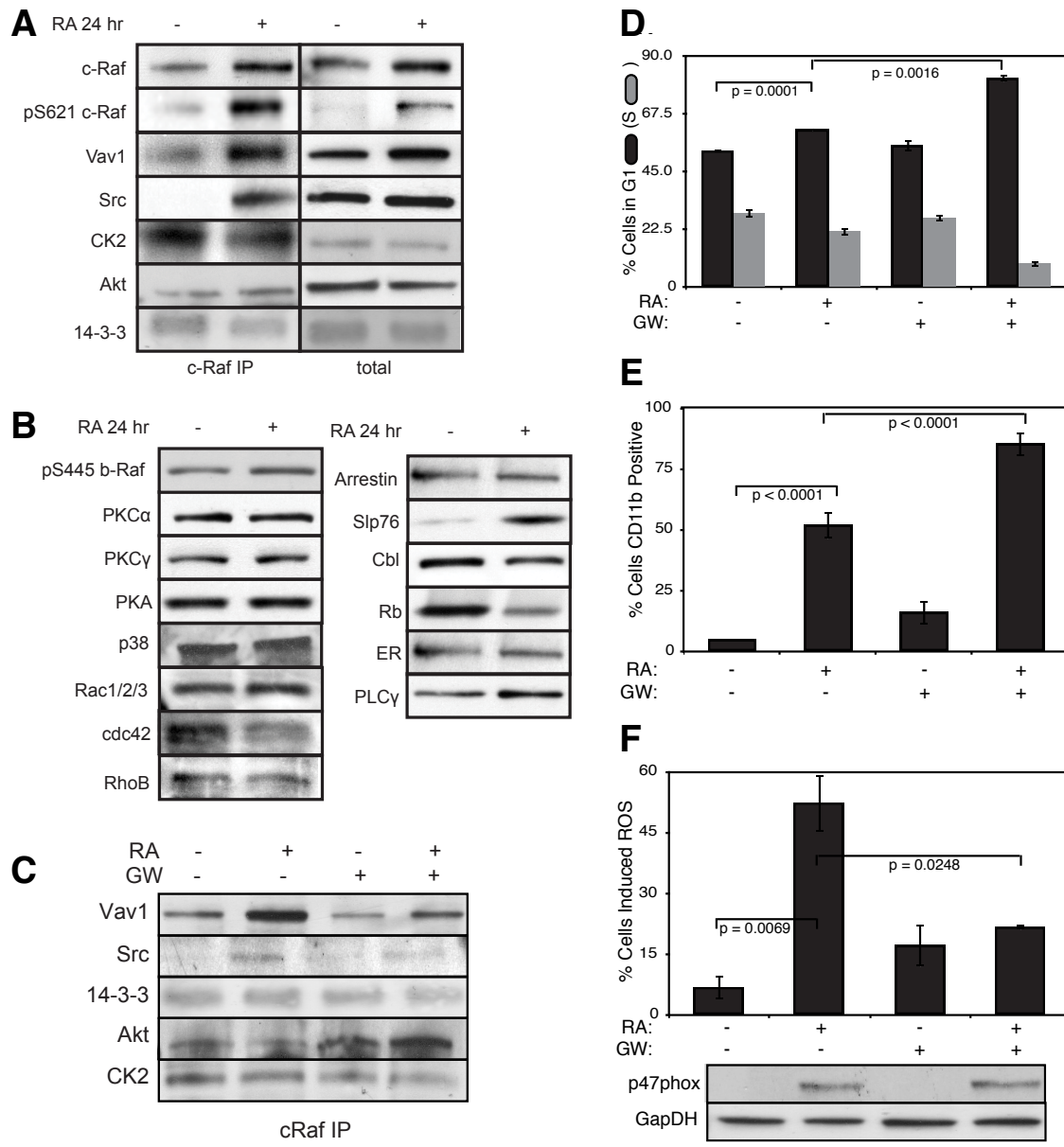


**Fig. 1:** Investigation of a panel of possible Raf interaction partners in the presence and absence of ATRA. A: Species identified to precipitate out with Raf: first column shows Western blot analysis on total Raf immunoprecipitation with and without 24 hr ATRA treatment and the second on total lysate. B: The expression of species considered that did not precipitate out with Raf at levels detectable by Western blot analysis on total lysate. C: Effect of the Raf inhibitor GW5074 on Raf interactions as determined by Western blot analysis of total Raf immunoprecipitation. The Authors note the signal associated with Src was found to be weak. D: Cell Cycle distribution as determined by flow cytometry indicated arrest induced by ATRA, which was increased by the addition of GW5074. E: Expression of the cell surface marker CD11b as determined by flow cytometry indicated increased expression induced by ATRA, which was enhanced by the addition of GW5074. F: Inducible reactive oxygen species (ROS) as determined by DCF flow cytometry. The functional differentiation response of ATRA treated cells was mitigated by GW5074.

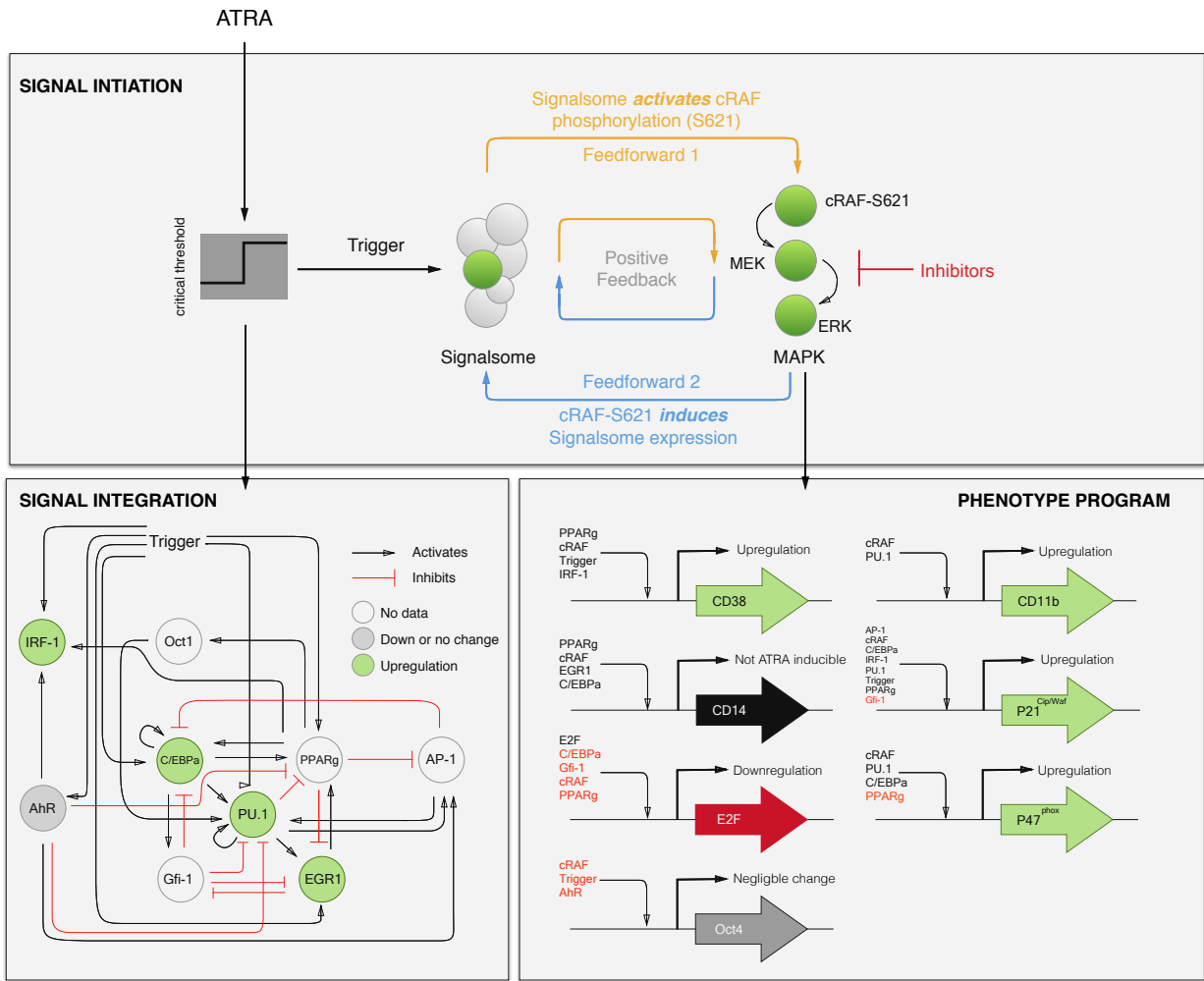


**Fig. 2:** Schematic of the effective ATRA differentiation circuit. Above a critical threshold, ATRA activates an upstream Trigger, which induces signalsome complex formation. Signalsome activates the mitogen-activated protein kinase (MAPK) cascade which in turn drives the differentiation program and signalsome formation. Both Trigger and activated cRaf-S621 drive a phenotype gene expression program responsible for differentiation. Trigger activates the expression of a series of transcription factors which in combination with cRaf-S621 result in phenotypic change.

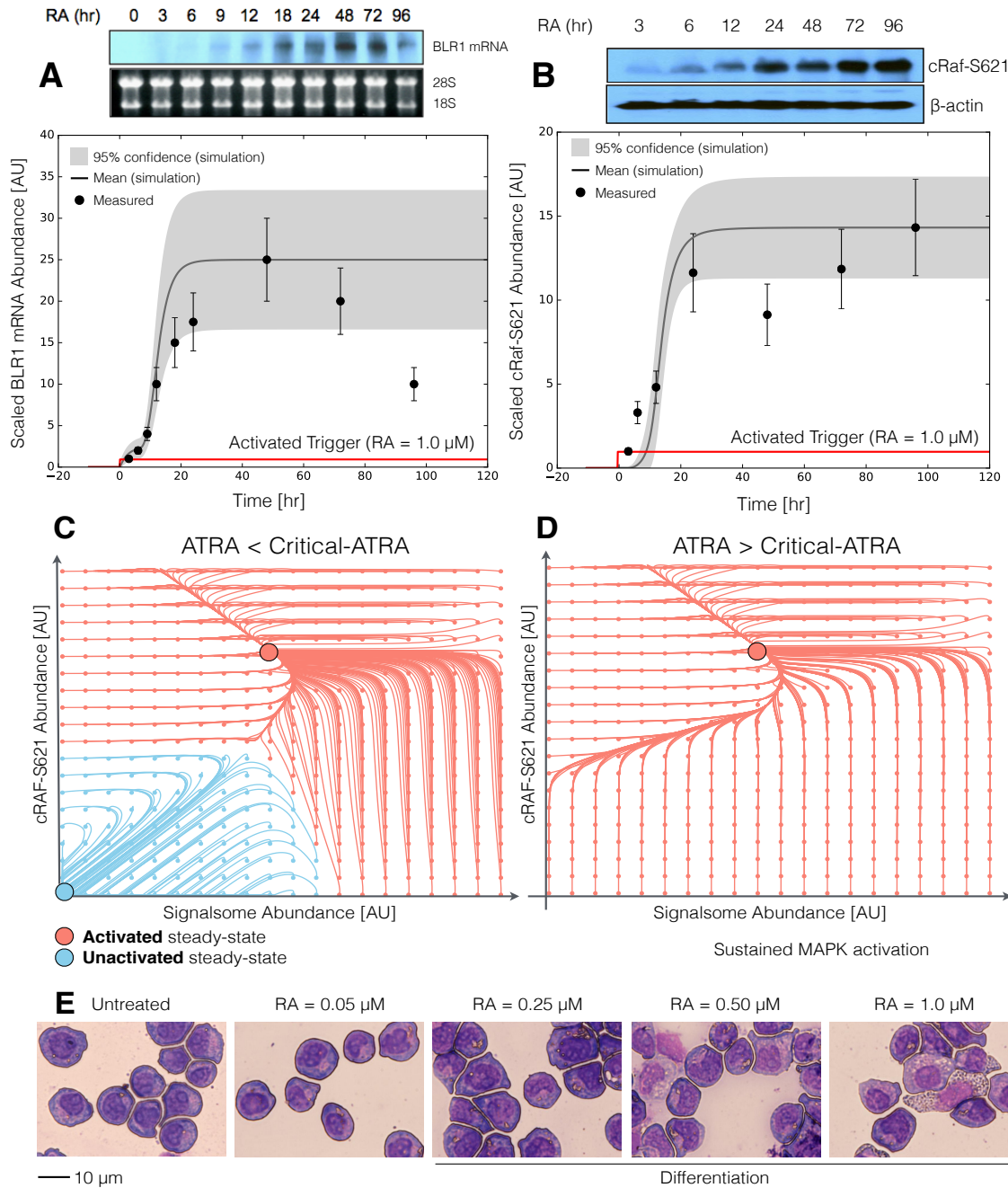


**Fig. 3:** Model analysis for ATRA-induced HL-60 differentiation. A: BLR1 mRNA versus time following exposure to 1  $\mu$ M ATRA at t = 0 hr. B: cRaf-pS621 versus time following exposure to 1  $\mu$ M ATRA at t = 0 hr. Points denote experimental measurements, solid lines denote the mean model performance. Shaded regions denote the 99% confidence interval calculated over the parameter ensemble. C: Signalsome and cRaf-pS621 nullclines for ATRA below the critical threshold. The model had two stable steady states and a single unstable state in this regime. D: Signalsome and cRaf-pS621 nullclines for ATRA above the critical threshold. In this regime the model had only a single stable steady state. E: Morphology of HL-60 as a function of ATRA concentration (t = 72 hr).

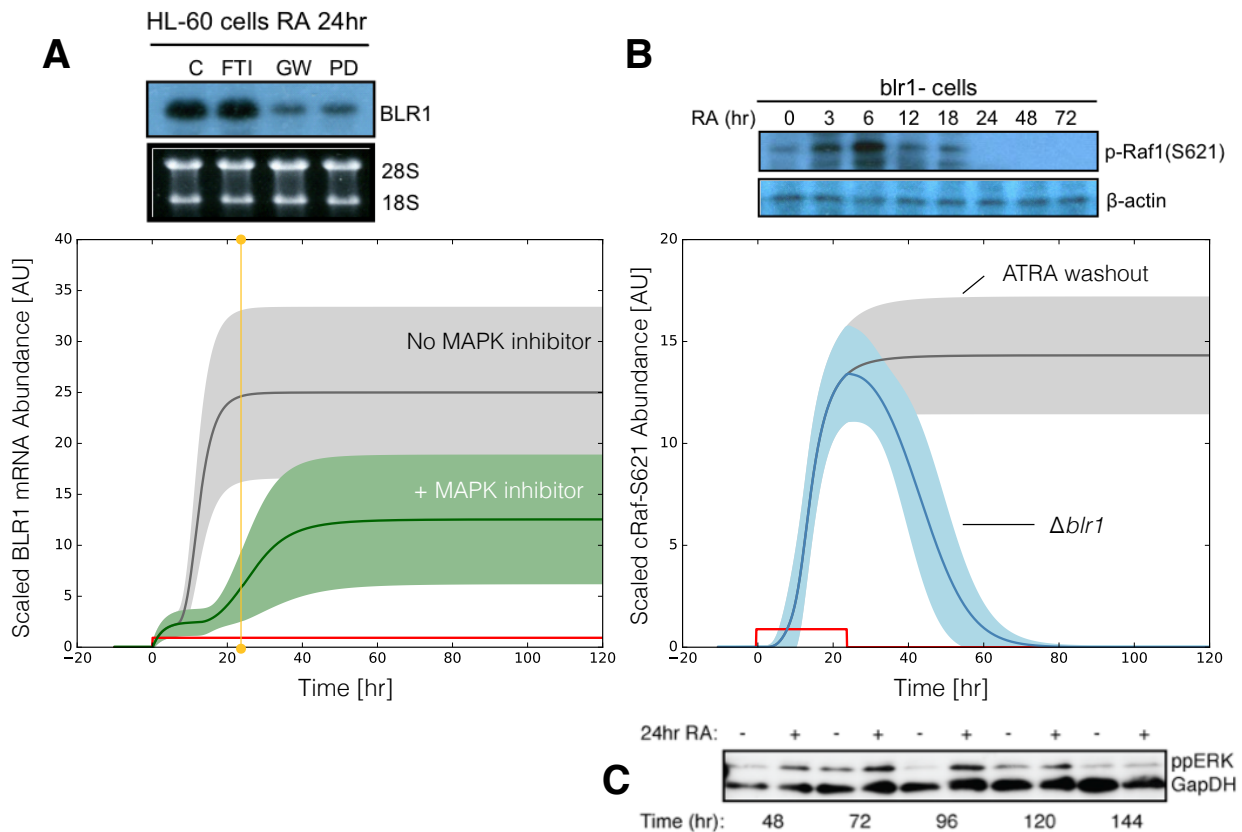


**Fig. 4:** Model simulation following exposure to  $1\mu\text{M}$  ATRA. A: BLR1 mRNA versus time with and without MAPK inhibitor. B: cRaf-pS621 versus time following pulsed exposure to  $1\mu\text{M}$  ATRA with and without BLR1. Solid lines denote the mean model performance, while shaded regions denote the 99% confidence interval calculated over the parameter ensemble. C: Western blot analysis of phosphorylated ERK1/2 in ATRA washout experiments. Experimental data in panels A and B were reproduced from Wang and Yen (20), data in panel C is reported in this study.

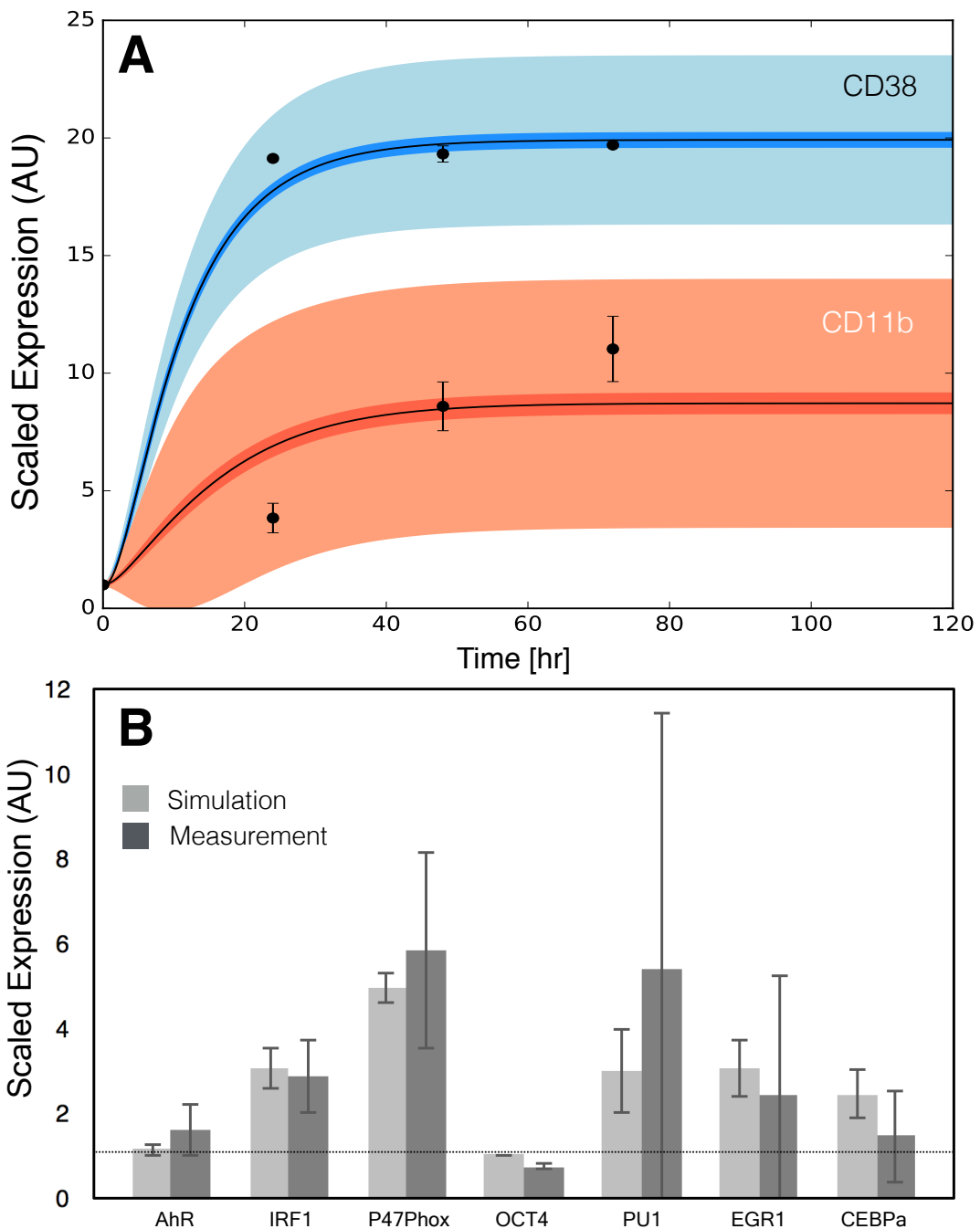


**Fig. 5:** Model simulation of the HL-60 gene expression program following exposure to  $1\mu\text{M}$  ATRA at  $t = 0$  hr. A: CD38 and CD11b expression versus time following ATRA exposure at time  $t = 0$  hr. B: Gene expression at  $t = 48$  hr following ATRA exposure. Experimental data in panels A and B were reproduced from Jensen et al. (48).